Influence of substrate configuration on the angular response pattern of infrared antennas

Jeffrey A. Bean*, Brian A. Slovick, Glenn D. Boreman

College of Optics and Photonics (CREOL), University of Central Florida, 4000 Central Florida Blvd., Orlando, FL 32816-2700, USA
* jbean@mail.ucf.edu

Abstract: The far-field angular response pattern for dipole antenna-coupled infrared detectors is investigated. These devices utilize an asymmetric metal-oxide-metal diode that is capable of rectifying infrared-frequency antenna currents without applied bias. Devices are fabricated on both planar and hemispherical lens substrates. Measurements indicate that the angular response can be tailored by the thickness of the electrical isolation standoff layer on which the detector is fabricated and/or the inclusion of a ground plane. Electromagnetic simulations and analytical expressions show excellent agreement with the measured results.

©2010 Optical Society of America

References and links

1. C. Balanis, *Antenna Theory: Analysis and Design* (John Wiley and Sons, Inc., New York, NY, 1996).
2. B. L. Coleman, "Propagation of Electromagnetic Disturbances Along a Thin Wire in a Horizontally Stratified Medium," Philos. Mag. **41**, 276 (1950).
3. C. Middlebrook, P. Krenz, B. Lail, G. D. Boreman, "Infrared Phased-Array Antenna," Microwave and Opt, Techn. Lett. **50**(4), 719–723 (2008).
4. F. González, and G. Boreman, "Comparison of dipole, bowtie, spiral and log-periodic IR antennas," Infrared Phys. Technol. **46**(5), 418–428 (2005).
5. C. Allen, F. Ardms, M. Wang, and C. C. Bradley, "Infrared-to-Millimeter, Broadband, Solid State Bolometer Detectors," Appl. Opt. **8**(4), 813–817 (1969).
6. P. M. Krenz, B. A. Lail, and G. D. Boreman, "Calibration of Lead-Line Response Contribution in Measured Radiation Patterns of IR Dipole Arrays," Accepted in IEEE J. Selected Topics Quant. Electron. **99** (2010).
7. H. J. Visser, *Array and Phased Array Antenna Basics* (John Wiley & Sons, Ltd., Chichester, West Sussex, England, 2005).
8. C. R. Brewitt-Taylor, D. J. Gunton, and H. D. Rees, "Planar Antennas on a Dielectric Surface," Electron. Lett. **17**(20), 729–731 (1981).
9. D. B. Rutledge, and M. S. Muha, "Imaging Antenna Arrays," in *IEEE Trans. on Antennas and Propagation* **AP-30** (4), 535–540 (1982).
10. B. Twu, and S. E. Schwarz, "Mechanism and Properties of Point-Contact Metal-Insulator-Metal Diode Detectors at 10.6 μ," Appl. Phys. Lett. **25**(10), 595–598 (1974).
11. S. M. Faris, T. K. Gustafson, and J. C. Wiesner, "Detection of Optical and Infrared Radiation with DC-Biased Electron-Tunneling Metal-Barrier-Metal Diodes," IEEE J. Quantum Electron. **9**(7), 737–745 (1973).
12. M. Heiblum, W. Shihyuan, J. R. Whinnery, and T. K. Gustafson, "Characteristics of Integrated MOM Junctions at DC and at Optical Frequencies," IEEE J. Quantum Electron. **14**(3), 159–169 (1978).
13. J. A. Bean, B. Tiwari, G. H. Bernstein, P. Fay, and W. Porod, "Thermal Infrared Detection Using Dipole Antenna-Coupled Metal-Oxide-Metal Diodes," J. Vac. Sci. Technol. B **27**(1), 11–14 (2009).
14. J. A. Bean, B. Tiwari, G. Szakmany, G. Bernstein, P. Fay, and W. Porod, "Antenna length and polarization response of antenna-coupled MOM diode infrared detectors," Infrared Phys. Technol. **53**(3), 182–185 (2010).
15. B. Slovick, P. Krenz, G. Zummo, and G. Boreman, "Evaporation of uniform antireflection coatings on hemispherical lenses to enhance infrared antenna gain," Infrared Phys. Technol. **53**(2), 89–93 (2010).
16. D. B. Rutledge, S. E. Schwarz, and A. T. Adams, "Infrared and Submillimetre Antennas," Infrared Phys. **18**(5-6), 713–729 (1978).
17. C. Fumeaux, M. Gritz, I. Codreanu, W. Schaich, F. González, and G. Boreman, "Measurement of the resonant lengths of infrared dipole antennas," Infrared Phys. Technol. **41**(5), 271–281 (2000).
18. P. Krenz, B. Slovick, J. Bean, and G. Boreman, "Alignment procedures for radiation pattern measurements of antenna-coupled infrared detectors," Opt. Eng. **49**(4), 033607 (2010).

19. E. Hecht, *Optics* (Addison Wesley Longman, Reading, MA, 1998).

1. Introduction

The radiation pattern of a transmitting antenna and by reciprocity, the angular response pattern of a receiving antenna, is dependent upon the type of antenna and its surroundings [1]. If an antenna is placed at the interface of two dielectrics, the pattern will differ from that of an antenna in free space due to the boundary conditions imposed on the electromagnetic fields [2]. By manipulating the substrate configuration of a receiving antenna, the angular response pattern can be modified in a controlled manner.

This paper studies the direct detection of a continuous wave incident beam through the use of a rectifying diode coupled to a dipole antenna. To study the effects of the substrate on the angular response pattern of infrared antennas, three different device configurations are considered: a planar substrate with an insulator layer above a ground plane, germanium hemispherical lens substrate with insulator layer, and the latter with an additional insulation layer and ground plane.

2. Background

The angular response patterns of infrared antennas have been investigated previously, but have mainly employed the use of microbolometers for detecting incident radiation [3, 4]. When subjected to infrared radiation, the temperature of the bolometer changes and consequently, so does its resistance [5]. Detection of incident infrared radiation is then measured using a constant voltage supply while monitoring the current flow through the bolometer. However, this yields a distributed response that receives contributions from both the antenna and lead structure, since the entire structure heats up due to the incident radiation. The bolometer is unable to distinguish the origin of the temperature change unless the temperature coefficient of resistance of the bolometer is much greater than the antenna and lead structures. This response due to non-antenna elements can be determined and the response calibrated [6], but can be mitigated altogether by replacing the microbolometer with a rectifying element, such as an MOM diode.

2.1 Dipole Antenna Angular Response

A half-wavelength dipole can be represented by two isotropic radiators, separated by one-half wavelength, which radiate equally in all directions [7]. The radiated fields possess a phase difference dependent on the spacing of these radiators and on the direction of radiation, which can result in constructive or destructive interference. Along the antenna axis, the phases of the radiated fields are separated by 180° due to the half wavelength spacing. These fields therefore cancel, giving rise to the fact that dipole antennas do not radiate along the antenna axis. However, in all directions perpendicular to and at the center of the antenna axis, there is no phase difference between the radiated fields because there is no spatial difference, and therefore their amplitudes add to the maximum. For all other directions, the radiated field amplitudes are between zero and the maximum. These field amplitudes, however, are altered if the antenna is placed at the interface of two materials. There, the antenna will radiate more strongly into the material with higher permittivity [8, 9]. Based on reciprocity, this means that a detector receives radiation preferentially from the material with the higher permittivity. This paper investigates the influence of the substrate configuration on the far-field angular response pattern for infrared antennas.

2.2 Antenna-coupled MOM Diode Infrared Detectors

Antenna-coupled MOM diodes have been shown to function as rectifying detectors from the long wave infrared (LWIR) [10] up to optical frequencies [11]. For a half-wavelength dipole at the resonant frequency, a maximum in the current distribution occurs at the center. When a MOM diode is located at the center of the dipole, incident radiation gives rise to Fermi level

modulation and rectification of resonant currents along the antenna [12]. If an asymmetric MOM diode is used, full functionality is achieved without biasing, providing for simplified circuitry and lower noise operation [13, 14].

3. Fabrication

Devices were fabricated on both planar substrates and the flat side of a hemispherical lens. For the planar substrates, a silicon wafer was coated with 100 nm of aluminum to form a ground plane and 1.6 µm of benzocyclobutene (BCB), which serves as an electrical insulation layer as well as a quarter-wave layer for 10.6 µm radiation. A thin standoff layer (47-475 nm) of SiO_2, which serves as an electrical insulation layer, was deposited on the flat side of the germanium hemispherical lens using electron beam evaporation. The curved surface was uniformly coated with a zinc sulfide quarter-wave anti-reflection coating using electron beam evaporation with a rotating stage [15].

Dipole antenna-coupled metal-oxide-metal (MOM) diode devices were patterned with electron beam lithography (EBL) and fabricated with a shadow evaporation procedure, which has been detailed in Refs. 13 and 14. EBL is chosen for the patterning of devices because of the small dimensions that are necessary for infrared detectors; the width of the dipole antennas must be less than 300 nm to promote longitudinal resonance [16] and the diode overlap area must be on the order of 100 x 100 nm to provide for rectification of 28.3 THz currents [17].

Aluminum was used for the base metal layer, which forms a native oxide in the presence of oxygen, and platinum is used to complete the MOM diode. The device consists of a dipole antenna with a MOM diode at the center, connected to direct current (DC) electrical leads, and is shown in Fig. 1. The dipole width is 100 nm and the $Al/AlO_x/Pt$ MOM diode overlap, which is approximately 75 x 75 nm, is shown in the inset image.
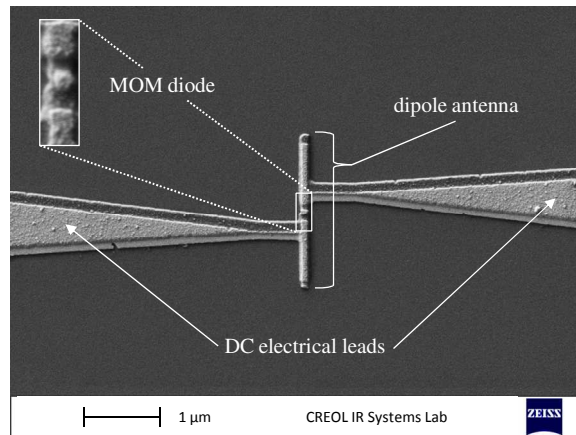

Fig. 1. Scanning electron micrograph of a dipole antenna-coupled MOM diode infrared detector. The dipole is 100 nm wide and 60 nm thick. Inset: detail of the MOM diode overlap area, which is approximately 75 x 75 nm.

4. Simulation and measurement

The material properties of the substrate and comprising materials of the device were characterized using an infrared ellipsometer to obtain layer thicknesses, refractive indices, and dielectric loss tangent. The device characteristics at 28.3 THz (10.6 µm) were used in the simulations to accurately model the device response to illumination from a CO_2 laser operating at 10.6 µm. Electromagnetic simulations for the fabricated devices were performed with Ansoft HFSS, using measured material properties. Analytical expressions based on the Fresnel coefficients were also used to compare the measured data and simulation results.

The devices were wire bonded into a chip carrier and placed on a goniometer stage with 8 degrees of freedom. The angular response pattern can be measured by placing the device at the axis of rotation of the goniometer and co-aligning to the laser beam. The output beam of the CO_2 laser is attenuated to a low power using neutral density filters, chopped with a mechanical chopper, and focused with F/8 optics to a near diffraction-limited spot size of approximately 230 µm. The devices were aligned using the method detailed by Krenz et al [18]. The devices were connected to low-noise current preamplifier, whose output is fed to a lock-in amplifier referenced to the frequency of the mechanical chopper. All measurements presented in this paper were measured without applying a bias on the device. It should be noted that the angular-response patterns measured in this manner are plotted on a scale linear in power.

4.1 Substrate-side Illumination through Hemispherical Lens and Insulating Film

The first set of devices were fabricated on a thin electrically insulating film of SiO_2 on top of the flat surface of a 10 mm diameter hemispherical immersion lens. A generic form of the cross-section of the device under test (DUT) and substrate is shown in Fig. 2. The arrow represents the propagation vector of a plane wave incident from the hemispherical substrate. In this case, the substrate is germanium and the film is SiO_2. The hemispherical lens is intended to replicate a dielectric half space. The center line of the incident beam remains normal to the curved surface throughout the angular pattern sweep. The laser beam is focused on the the device and the polarization of the electric field of the incident radiation is parallel to the antenna since a dipole responds to the parallel component of the electric field. The antenna is rotated about its axis to produce the H-plane angular pattern.
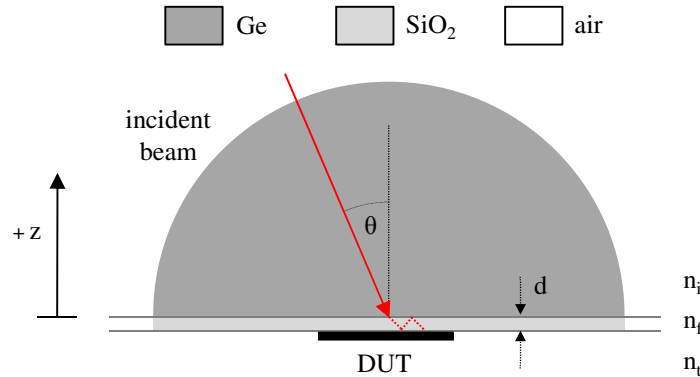

Fig. 2. Cross sectional illustration of a device fabricated on a thin insulating film on a germanium hemispherical lens. The hemispherical lens is very large compared to the wavelength of incident radiation, while the thickness of the SiO_2 film is very small compared to the incident wavelength. The incident beam is normal to the curved surface and consequently aligned with the device at the center of the lens.

Previous research has shown that the electric field at the dipole on the interface is equal to the incident field times the transmission coefficient [8]. The fraction of the incident power that reaches the antenna will be proportional to the squared norm of the transmission coefficient for the interface on which the antenna is fabricated. The film can be regarded as a Fabry Perot cavity with a transmission coefficient [19]

$$t = \frac{(1+r_{tf})(1-r_{if})e^{-i\delta}}{1-r_{tf}r_{if}e^{-i2\delta}},$$

(1)

where r_{tf} is the reflection coefficient at the bottom interface in Fig. 2, r_{if} is the reflection coefficient at the top interface, and δ is the phase shift due to propagation in the film layer, calculated as

$$\delta = \frac{2\pi}{\lambda_0} d \sqrt{n_f^2 - n_i^2 \sin^2 \theta}. \tag{2}$$

where λ_0 is the wavelength of incident radiation in free space, d is the thickness of the film, n is the refractive index of the respective material, and θ is the angle of arrival. The thickness d is taken to be negative since the angle of arrival is measured relative to the film-air interface, not the substrate-film interface. The reflection coefficients r_{12} in Eq. (1) are given by

$$r_{12} = \frac{n_1 \cos\theta - \sqrt{n_2^2 - n_1^2 \sin^2 \theta}}{n_1 \cos\theta + \sqrt{n_2^2 - n_1^2 \sin^2 \theta}}. \tag{3}$$

The angular response pattern in the H-plane is shown in Fig. 3 for a 3.1 μm half-wavelength dipole on a 47 nm layer of SiO$_2$ illuminated through the germanium hemispherical lens. The rectified current of the MOM diode is proportional to the optical power at the MOM diode and as such, the squared norm $|t|^2$ represents the angular response pattern of the device. The red data points indicate the measured data, the solid blue line indicates the HFSS simulation, and the dotted black line plots the squared norm $|t|^2$ of the transmission coefficient shown in Eq. (1).
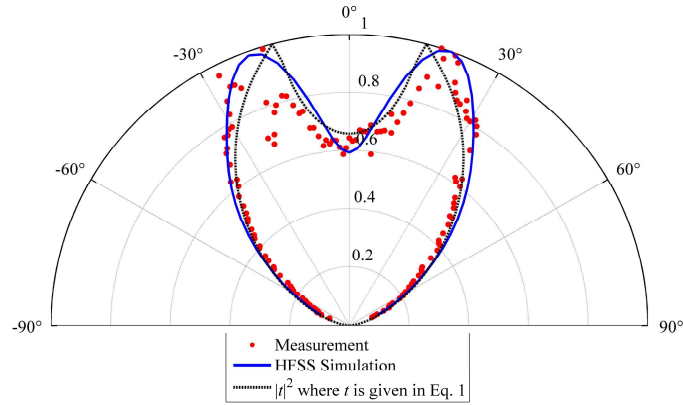

Fig. 3. H-plane angular response pattern of dipole ACMOMD on 47 nm film of SiO$_2$. The critical angle between Ge and air is approximately 15°, where the peak angular response is measured.

The measured data closely follows the expected trend from both the HFSS simulation and the norm squared of the transmission coefficient, with the peaks in the H-plane response occuring at angles slightly larger than critical angle. The full-width half-maximum (FWHM) beam width is approximately 90°. For such a thin film of SiO$_2$, the pattern approaches that of a dipole directly on the hemispherical lens.

Figure 4 shows the angular response pattern in the H-plane for a dipole antenna identical to the one in Fig. 3, on a 169 nm layer of SiO$_2$. Again, the device is illuminated through the substrate.
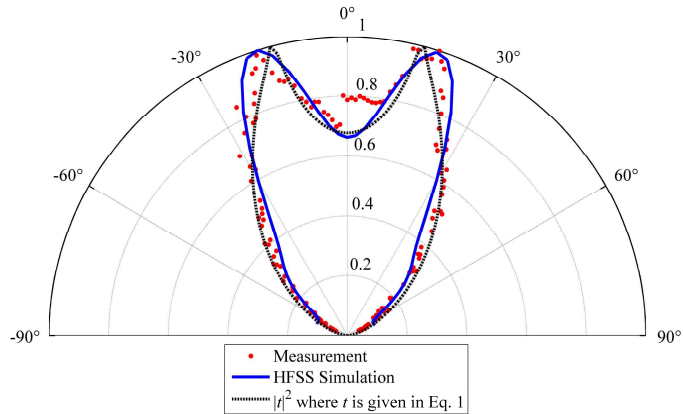
Fig. 4. H-plane angular response pattern of dipole ACMOMD on 169 nm film of SiO_2. The peak angular response is at approximately 15°, which is the critical angle between Ge and air.

Excellent agreement is observed between the measured data and the simulation from HFSS, as well as the norm squared of the transmission coefficient. The peaks in the H-plane response correspond to the cricitcal angle between the SiO_2-air interface. The pattern is narrower than the case with the 47 nm layer SiO_2 layer, with a FWHM of approximately 75°. It is believed that imperfections in the antireflection coating on the curved surface of the hemispherical lens cause the deviations seen in the data near broadside.

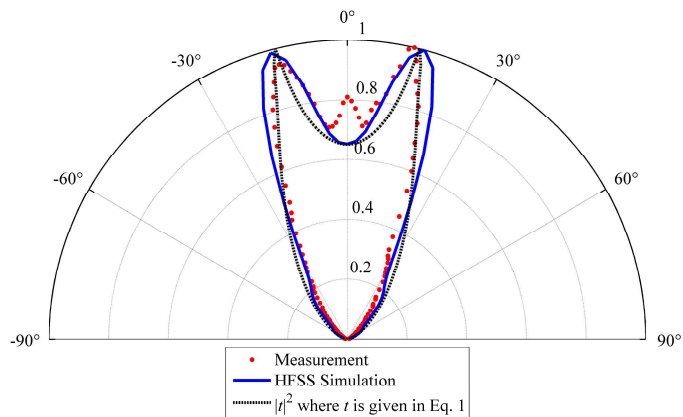Figure 5 shows the same device geometry fabricated on a 475 nm layer of SiO_2.

Fig. 5. H-plane angular response pattern of dipole ACMOMD on 475 nm film of SiO_2. Again, the peak angular response is measured at the Ge/air critical angle.

Again, the measured data matches up with the simulation result from HFSS and the norm squared of the transmission coefficient. The pattern is further narrowed from the 169 nm SiO_2 layer case, to approximately 50° FWHM. Again, the difference between the measured pattern and theoretical is due to imperfections in the antireflection coating. It was found that increasing the SiO_2 thickness beyond 475 nm did not further narrow the pattern, but instead lowered the broadside response. Figure 3, Fig. 4, and Fig. 5 show that the radiation pattern is essentially unchanged for angles below the critical angle.

The narrowing of the pattern can be explained by the interference between the radiation incident on the device and that reflected from the Ge/SiO_2 interface. Only the first reflected wave is shown in Fig. 2. The optical path length difference between the waves depends on the film thickness and the angle of incidence. For very thin films (47 nm), the phase difference is negligible and the angular response pattern resembles that of a dipole antenna on germanium.

As the film thickness increases, the degree of destructive interference increases, leading to a narrowed pattern. Although the effective index changes for the different SiO$_2$ standoff layer thicknesses, a 3.1 µm half-wavelength dipole antenna was used in each case. The antenna length impacts the magnitude of the device response, but the shape of the angular response pattern is not dependent of the dipole length.

4.2 Air-side Illumination on Insulator Above Ground Plane

The next set of devices was fabricated on a planar substrate with a 1.6 µm layer of BCB above a 100 nm aluminum ground plane on a silicon wafer as a mechanical support. A cross-section of the DUT and substrate is shown in Fig. 6. The device responds to incident radiation from the air side as well as the refelected wave in the BCB from the ground plane.
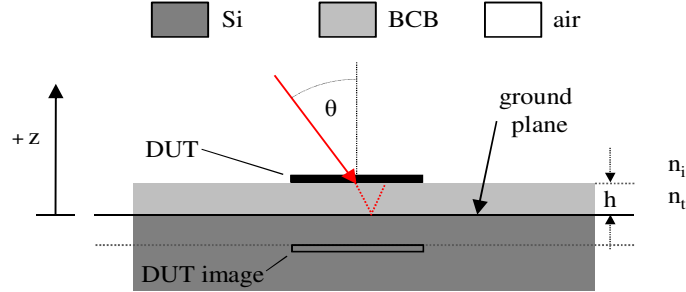

Fig. 6. Cross-sectional view of devices fabricated on a planar substrate with a 1.6 µm layer of BCB above a ground plane, illuminated from the air side. The device responds to radiation from both the air side and the DUT image reflected from the ground plane. As such, a quarter-wave layer of BCB was chosen.

The angular response pattern of a dipole above a ground plane is proportional to the product of the antenna pattern for the dielectric interface and an inteference factor to account for the image of the dipole that is generated by the ground plane [6]. In this case, the effective transmission coefficient t_{GP} is given by

$$t_{GP} = t\left[1 + \exp(i\phi)\right]. \tag{5}$$

where φ is the phase shift due to propagation in the layer below the device

$$\phi = \frac{4\pi h}{\lambda_0}\sqrt{n_t^2 - n_i^2 \sin^2\theta} \pm \pi. \tag{6}$$

and h is the thickness of the insulator, which in this case is BCB, and the π phase accounts for the reflection from the ground plane. In this case, there is no film present above the device as in Fig. 2. To simplify the expression, the ground plane factor only accounts for the first reflected wave.

The measured angular response of a 3.4 µm half-wavelength dipole in the H-plane is shown in Fig. 7. The data points indicate the measured data, the solid blue line indicated the HFSS simulation, and the dotted black line indicates the norm squared of the transmission coefficient in Eq. (1), where $n_s = 1$ for air-side illumination, $d = 0$ µm, and $n_a = 1.55$ for BCB, and includes the ground plane image factor, where $h = 1.6$ µm and $n = 1.55$ for BCB. The device responds to incident radiation from the air side as well as the wave refelected from the ground plane.
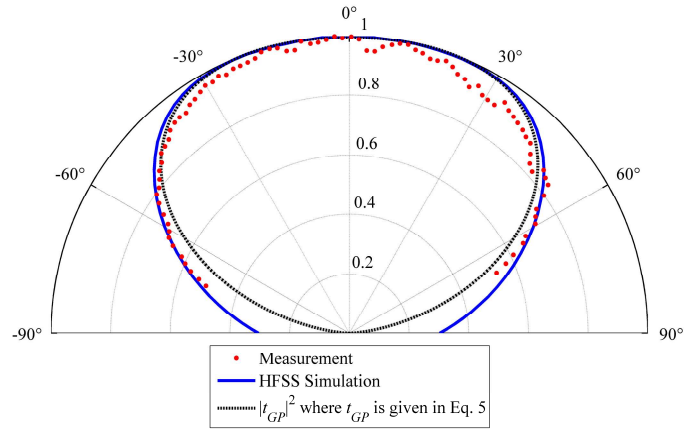
Fig. 7. H-plane angular response pattern for dipole device on 1.6 µm BCB microcavity above a ground plane.

The measured data shows agreement to the HFSS simulation and the norm squared of the transmission coefficient with the ground plane image factor. A dipole antenna on the ground plane yields the broadest angular response pattern in the H-plane, with a FWHM of approximately 140°.

4.3 Substrate-side Illumination on Insulating Film with Ground Plane

The two cases shown in sections 4.1 and 4.2 can also be combined. In this case, a half-wavelength dipole 3.1 µm in length was fabricated on a 475 nm SiO_2 layer on a germanium hemispherical substrate. The device was then covered in a 900 nm layer of SiO_2 and then 100 nm of aluminum. An illustration of the cross-section of this substrate and DUT is shown in Fig. 8.
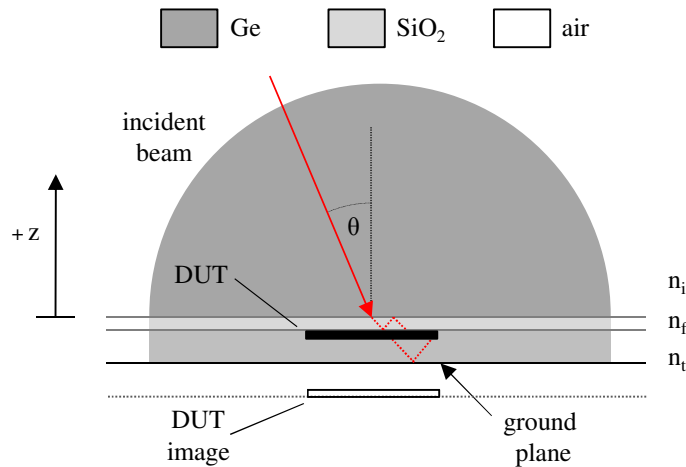

Fig. 8. Cross-sectional view of devices fabricated on a germanium hemispherical substrate with a 475 nm layer of SiO_2 and then covered with a layer of SiO_2 and an aluminum ground plane. This device is illuminated through the germanium half-space. The device responds to radiation incident from the germanium hemisphere and that reflected from the ground plane.

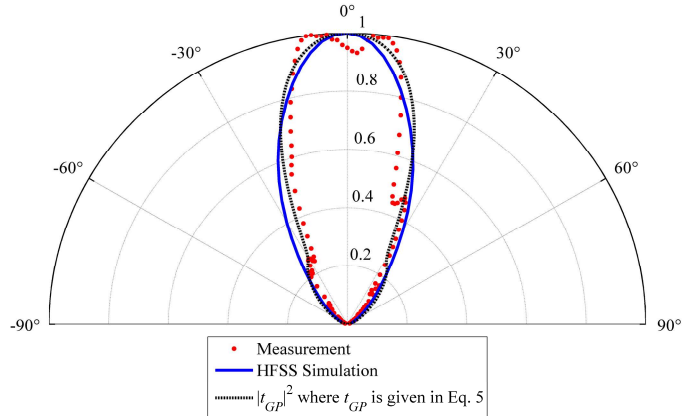The angular response pattern in the H-plane is shown in Fig. 9.

Fig. 9. H-plane angular response pattern of dipole antenna on 475 nm film of SiO_2 below 0.9 µm SiO_2 layer with ground plane.

The analytical expression in this case is the sqaured norm of the transmission coefficient t_{GP} shown in Eq. (5), which matches the measured data quite well. The FWHM is approximately 40-50°. There is good agreement between the HFSS simulation and the analytical expression. It is believed that film adhesion issues for the bottom SiO_2 layer are responsible for the the small deviations from the expected response.

5. Discussion

The simulations and measurements demonstrate the influence of the substrate configuration on the H-plane angular response pattern of a dipole antenna. For substrate-side illumination through a hemispherical immersion lens with a thin SiO_2 standoff layer (50 nm), the angular response pattern is similar to that of an antenna directly on germanium. As the thickness of the insulation layer increases, the pattern narrows.

For an insulating layer above a ground plane, the angular response pattern of a dipole is broadened compared to the case where no ground plane is present. This is due to reflections from the ground plane, which add constructively with the incident radiation at large angles when the microcavity approaches one quarter wave thick, which is approximately 2.0 µm.

The last configuration has the device fabricated on a SiO_2 standoff layer on top of a germanium hemispherical lens and capped by a quarter-wave matching layer and ground plane. This FWHM was very similar to the case without the ground plane.

6. Conclusions

The paper has demonstrated control of beam width and angular response pattern by manipulating the surroundings of the antenna. The H-plane angular response of a dipole antenna can be broadened by the use of a ground plane and narrowed through the use of an electrically isolating standoff layer. The thickest SiO_2 layer (475 nm) showed the narrowest angular response pattern for a dipole device. Agreement between the measured angular response patterns and the electromagnetic predictions indicate that the measured response is solely due to the antenna structures and the currents rectified by the MOM diode, and not to the electrical leads or surrounding circuitry.